Chapter 1 *Introduction & Literature reviews*

1.1 Perovskite

In 1839, Gustav Rose made the initial discovery of the perovskite mineral in the Ural Mountains of Russia, which bears the chemical formula $CaTiO_3$. After Lev Perovski, a Russian mineralogist, its named as perovskite. The word "perovskite" refers to compounds having the general formula ABO_3, where A stands for a trivalent rare earth metal (La, Gd, Pr, Ho, etc.) or a divalent alkali earth (Ca, Sr, Ba, etc.) and B stands for a trivalent/tetravalent transition metal (Mn, Cr, Fe, Co, Ti, etc.). The ideal perovskites ABO_3 are cubic in structure with Pm3m space group [1]. Perovskite (ABO_3) is frequently described as having a cubic structure with B-cations located at the center of the oxygen octahedra (BO_6) and A-cations located at the cube's corner (figure 1.1(a)). Figure 1.1(b) and (c) depict the arrangement, showing that the A cation is surrounded by twelve oxygen anions (AO_{12}), whereas the B cation is surrounded by six oxygen anions (BO_6). [1–3].

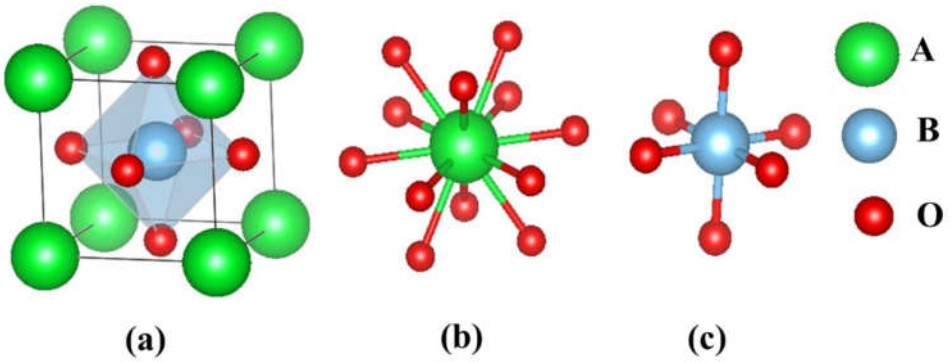

Figure 1.1 (a) ABO_3 Ideal cubic perovskite structure (b) cuboctahedra AO_{12} and(c) octahedra BO_6.

As the degrees of freedom for spin, electric charge, and lattice are strongly coupled, perovskite compounds exhibit a variety of uncommon and complex characteristics [2]. Typically, materials such as manganites, orthoferrites, orthochromites, cobaltites, and other exhibit a perovskite structure and are known to crystallize in an orthorhombic structure. Although these materials have similar crystal structure, their magnetic properties are heavily influenced by the electronic configuration of both the rare earth (R) and transition metal (TM) ions. These compounds have drawn a lot of attention because doping at either the A-site or the B-site can change their physical characteristics. Additionally, the structural distortion and electronic structure of the compound can be altered based on the ionic size of the replaced element, allowing engineers to control the complex's electrical, optical, thermal, and magnetic properties [1]. The structure of perovskite compounds is typically influenced by the size ratio of the elements that are incorporated. The ionic radii of the A-site cations in a perovskite ABO_3 structure are ideally greater than those of the B-site cations and similar in size to oxygen anions.

Goldschmidt's tolerance factor (GTF), which is a measure of distortion in crystal structure, can be used to quantify the distortion in system, which generally defined as [4]

$$t = \frac{R_A + R_O}{\sqrt{2}(R_B + R_O)} \tag{1.1}$$

where R_A, R_B, and R_O are the corresponding ionic radii of the A and B cations and the oxygen anion. For a perfect cubic perovskite, the value of "t" is unity; however, for a deformed perovskite, it would be less than unity ($t < 1$). For stable perovskite compounds, the value of "t" falls between the ranges of 0.8 and 1.0.

Incorporation of various chemical element at distinct site results in a deviation of perovskite structure from its ideal cubic structure. Numerous research groups have given a lot of contribution on the study of various distortions and their effect on crystal symmetry [1,5–10]. The literature commonly describes the three different types of distortion.

1. Displacement of cation A and B from its position.
2. Distortion in BO_6 octahedra.
3. Rotation of BO_6 octahedra.

Due to flexible nature of the perovskite structure, there are instances where multiple distortions coexist. These distortions reduce the symmetry of the cubic structure and lead to unique properties, such as colossal magneto-resistance [11–13], superconductivity [14–16], and multiferroicity [17–19].

1.2 Magnetism

From basic research on quantum mechanics, it has been revealed that magnetism primarily arises from the spin of electrons and their exchange interactions. This enhanced understanding of magnetic properties has opened up opportunities for incorporating magnets into advanced devices for everyday use.

1.2.1 Fundamental Theory of Magnetism

The behavior of electron inside atoms is the source of magnetism. Two types of magnetic moments, namely orbital magnetic moment and intrinsic spin moment, independently contribute to the overall magnetism of a material. As a result, all atoms with at least one electron exhibit some form of magnetism, even though only molecules and atoms with

unpaired electrons exhibit useful magnetic behavior. This is due to Pauli's exclusion principle, which states that an orbital can accommodate a maximum of two electrons with anti-parallel spins, thereby canceling each other's magnetic moments. Transition metals like manganese, cobalt, nickel, and iron, which possess unpaired d-electrons, are common examples of magnetic materials that exhibit spontaneous magnetization. The magnetic properties of these elements primarily arise from the exchange interaction between electrons. Rare earth elements, including gadolinium, neodymium, europium, samarium, and cerium, also display magnetic properties due to their unpaired f-electrons. In the case of rare earth metals, both spin and orbital motion significantly contribute to their magnetic characteristics. Additionally, compounds, metal oxides, and alloys consisting of transition metals and rare earth metals also exhibit strong magnetic properties.

1.2.2 Types of Magnetism in Perovskites

Magnetic materials can be classified based on the interaction between their magnetic moments as follows [20].

1. Diamagnetism
2. Para-magnetism
3. Ferromagnetism
4. Anti-ferromagnetism
5. Ferrimagnetism

1.2.2.1 Diamagnetism

When a magnetic material is exposed to an external magnetic field, the orbital motion of electrons within the material is affected in such a way that it produces an induced magnetic moment that opposes the applied magnetic field (in accordance with Lenz's law). This induced diamagnetic moment will continue to exist as long as the material remains under the influence of the external magnetic field [21].

1.2.2.2 Para-magnetism

Paramagnetic materials possess unpaired electron spins that generate a magnetic moment. In the absence of an external magnetic field, the magnetic moments are randomly oriented as shown in figure 1.2. The magnetization of a paramagnetic material is proportional to the applied magnetic field strength (H) and inversely proportional to the absolute temperature (T) [22]. Curie law describes the temperature-dependent susceptibility of paramagnetic materials, where the susceptibility is determined by the number (N) of magnetic moments per unit volume, each having a magnetic moment of μ.

$$\chi = \frac{\mu_o N \mu^2}{3k_B T} = \frac{C}{T} \qquad ---(1.2)$$

where C is a Curie constant and specific to each material and k_B is the Boltzmann's constant. The modified Curie law (Curie-Weiss law) is given by

$$\chi = \frac{C}{T - \theta} \qquad ---(1.3)$$

The symbol θ denotes the Curie temperature, which can take on positive, negative, or zero values. A positive value of θ signifies that the material exhibits ferromagnetism below a specific temperature, and the magnitude of θ represents the transition temperature (Curie

temperature, T_C). Conversely, a negative value of θ indicates that the material displays antiferromagnetism below a specific temperature, and the magnitude of θ represents the transition temperature (Néel temperature, T_N). Some instances of paramagnetic materials include salts of transition elements and oxides of rare earths elements [20].

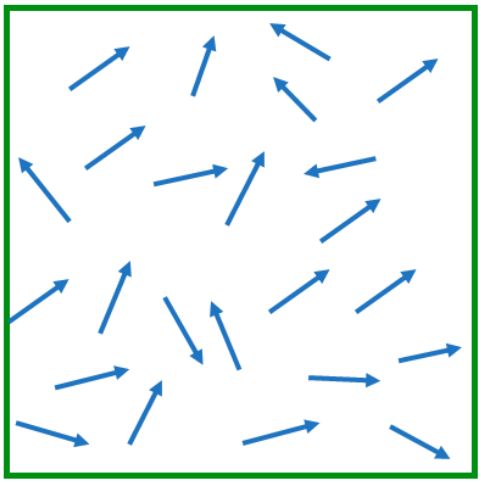

Figure 1.2 In the absence of an external applied field, a schematic illustration of magnetic dipole moments in paramagnetic material.

1.2.2.3 Ferromagnetism

Ferromagnetic materials display spontaneous magnetization within their domains and exhibit cooperative behavior. All the magnetic moments in ferromagnetic materials are oriented in a single direction, as depicted in figure 1.3. To understand this phenomenon, Weiss proposed a molecular field theory, which suggests that the magnetic moments within the domains of ferromagnetic materials align parallel to each other below T_C [23]. This alignment is caused by the presence of a molecular field $B = \lambda M$, where λ represents the molecular field constant, and M is the spontaneous magnetization of the material. Examples of ferromagnetic materials include transition metals such as Ni, Fe, and, Co which have T_C values of 631 K, 1043 K, and, 1394 K, respectively [20].

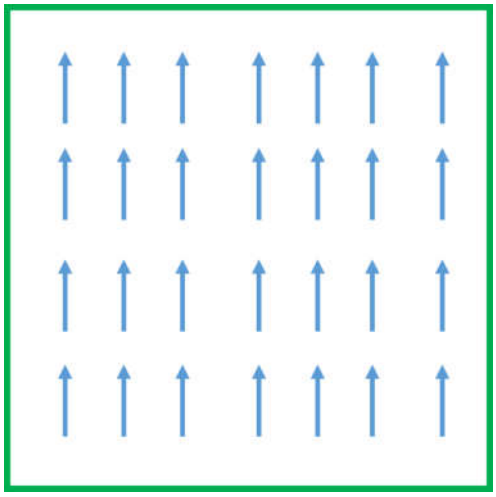

Figure 1.3 A schematic illustration of ferromagnetic material's magnetic dipole moments aligned in one direction.

1.2.2.4 Anti-ferromagnetism

AFM materials exhibit a magnetic phenomenon where the adjacent magnetic moments, which have equal magnitudes, align antiparallel to each other below the Néel temperature (T_N) as shown in figure 1.4. This results in a zero net magnetization.

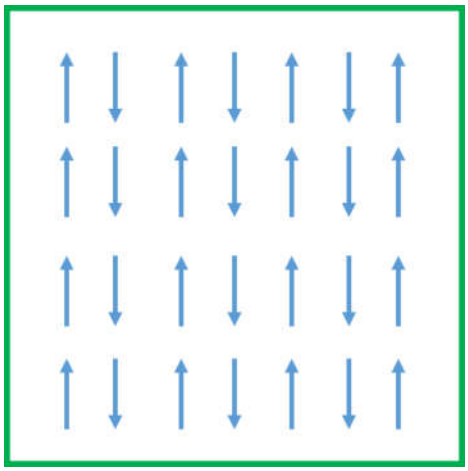

Figure 1.4 Schematic illustration of an antiferromagnetic material's magnetic dipole moment that is aligned in the opposite direction.

As the temperature increases above T_N, these materials exhibit similar behavior to that of paramagnets. In addition, AFM materials exhibit a small and positive susceptibility. The equation 1.3 and figure 1.5 illustrate how the inverse susceptibility of para-, ferro-, and antiferro-magnetic materials can be visualized. Examples of AFM materials and their respective Néel temperatures are as follows: FeMn (67 K), FeO (116 K), MnO (116 K), CoO (292 K), and, Cr_2O_3 (307 K). [20].

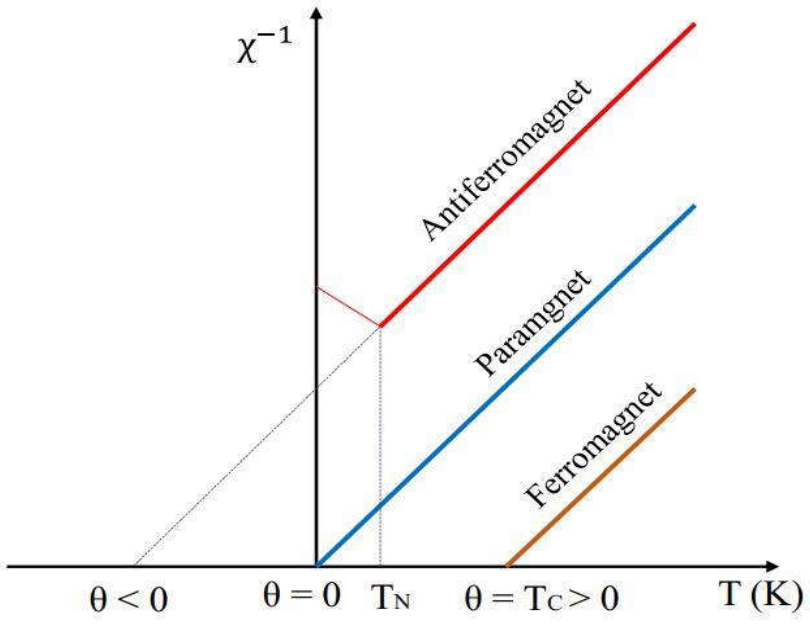

Figure 1.5 Temperature-dependent variation in the reciprocal of magnetic susceptibility for para-, ferro-, and antiferromagnetic materials.

Besides what has been mentioned earlier, perovskite compounds also exhibit anti-ferromagnetic behavior. Normally, materials that display AFM characteristics have zero net magnetization, as previously discussed. However, in certain cases, the slight tilt of magnetic moments, known as canted nature, generates a small net magnetization. Perovskite oxide compounds with Pnma space group exemplify canted antiferromagnets, with a spin canting

that is perpendicular to the spin easy axis [24]. Depending on the magnetic interaction among moments in the magnetic unit cell, different types of AFM ordering can occur, as illustrated in figure 1.6.

There are several types of anti-ferromagnetic (AFM) ordering, including [25,26]:

1. A-type: In this type, the magnetic moments in the same plane are ferromagnetically coupled, while the inter-plane coupling is anti-ferromagnet ic.
2. C-type: Here, the magnetic moments in the same plane are anti-ferromagnetically coupled, while the inter-plane coupling is ferromagnetic.
3. G-type: In this type, the coupling of magnetic moments is anti-ferromagnetic both in intra-plane and inter-plane directions.

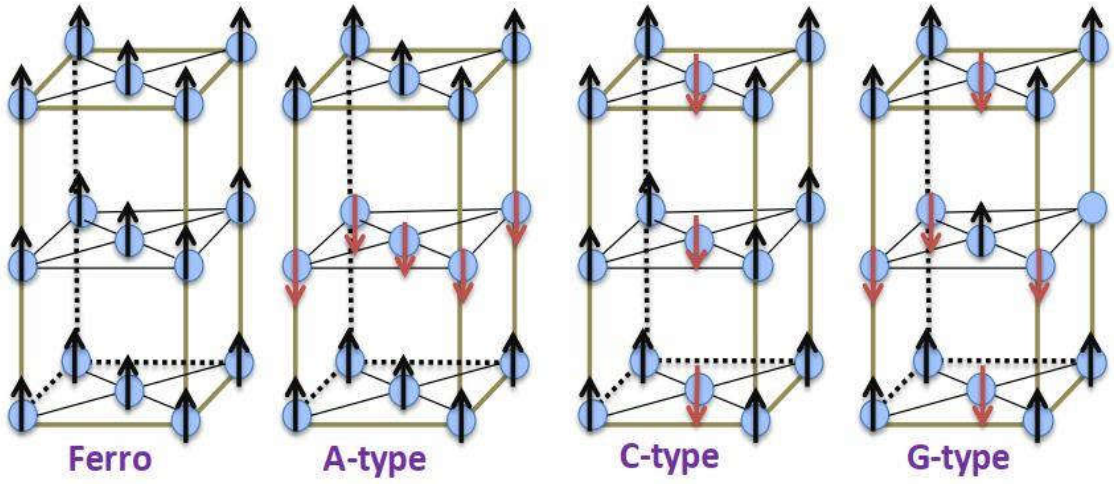

Figure 1.6 Classification of AFM ordering [25,26] .

These AFM materials coupling with ferromagnetic sublattice can cause spin pinning at interface which gives rise to a significant phenomenon called exchange bias (EB). This distinctive characteristic of the AFM/FM sublattices has potential applications in spintronics and data storage devices.

1.2.2.5 Ferrimagnetism

Ferrimagnetic materials will have their magnetic moments aligned in an anti-ferromagnetic way, but with different sublattice magnitudes, leading to a net magnetization as shown in figure 1.7. Numerous examples of ferrimagnetic materials exist, such as $Gd_3Fe_5O_{12}$, $NiFe_2O_4$, $Ho_3Fe_5O_{12}$, Fe_3O_4, $CoFe_2O_4$ and $MnFe_2O_4$ [22].

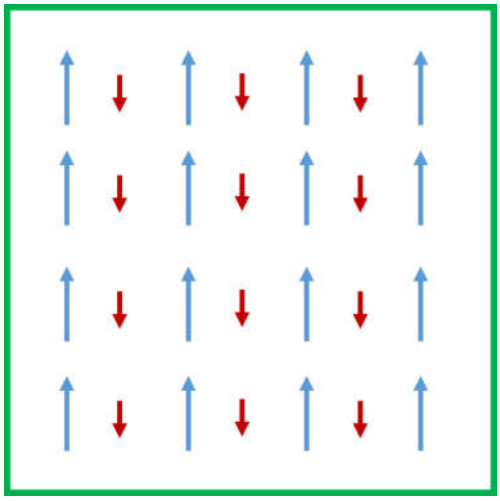

Figure 1.7 Diagram illustrating the alignment of magnetic dipole moments in a ferrimagnetic material in opposite directions.

1.3 Magnetic interaction

Magnetic interaction is a fundamental concept in the study of magnetic materials. According to research, the magnetic properties of any magnetic material are determined by the strength of the exchange interactions between the magnetic moments associated with the ions in the material [22]. These exchange interactions are separated in two categories: (1) direct exchange and (2) indirect exchange (super-exchange, double exchange, and Dzyaloshinskii-Moriya (DM) interaction).

1.3.1 Direct exchange interaction

The exchange energy, an essential component of the total energy in molecules and the formation of covalent bonds in solids, is defined by Heisenberg as [20,22]

$$E_{ex} = -J_{ex} S_i S_j \cos\theta \qquad \text{--------(1.4)}$$

Here, S_i and S_j represent the electronic spins at the i^{th} and j^{th} atomic sites, respectively, taking values of +1/2 or -1/2. J_{ex} denotes the exchange integral, and θ represents the angle between the two spins. The value of cos θ is 1 when the spins are parallel and -1 when they are antiparallel. For ferromagnetic materials, J_{ex} is positive, whereas for antiferromagnetic materials, it is negative. These exchange forces govern the emergence of ferromagnetism and anti-ferromagnetism in materials. The Bethe-Slater plot, shown in figure 1.8, illustrates the relationship between the sign and magnitude of J_{ex} and the interatomic distance. The plot reveals that J_{ex} is positive for ferromagnetic materials and negative for antiferromagnetic materials. This exchange interaction occurs between closely spaced ions with overlapping wave functions. The overlapping charge density lobes of adjacent single free atoms, residing next to each other, contribute to different states. The overlap region of charge density arises from these lobes, resulting in strong short-range coupling, which rapidly diminishes as the separation between magnetic ions increases. In the case of direct exchange interaction, the exchange integral (J_{ex}) can be either positive or negative, depending on the balance between kinetic and coulombic energies. When two atoms each have a single electron, the coulombic interaction is minimized when they are in close proximity, and the electrons spend most of their time between the nuclei. Due to Pauli's exclusion principle, these electrons must have

antiparallel spins since they prefer to occupy the same position in space simultaneously. This antiparallel alignment gives rise to antiferromagnetic ordering and, consequently, a negative value of the exchange interaction J_{ex}. On the other hand, when the atoms are far apart, the electrons spend more time away from each other, reducing the electron-electron Coulombic interaction. This scenario can lead to parallel alignment of spins, resulting in ferromagnetic

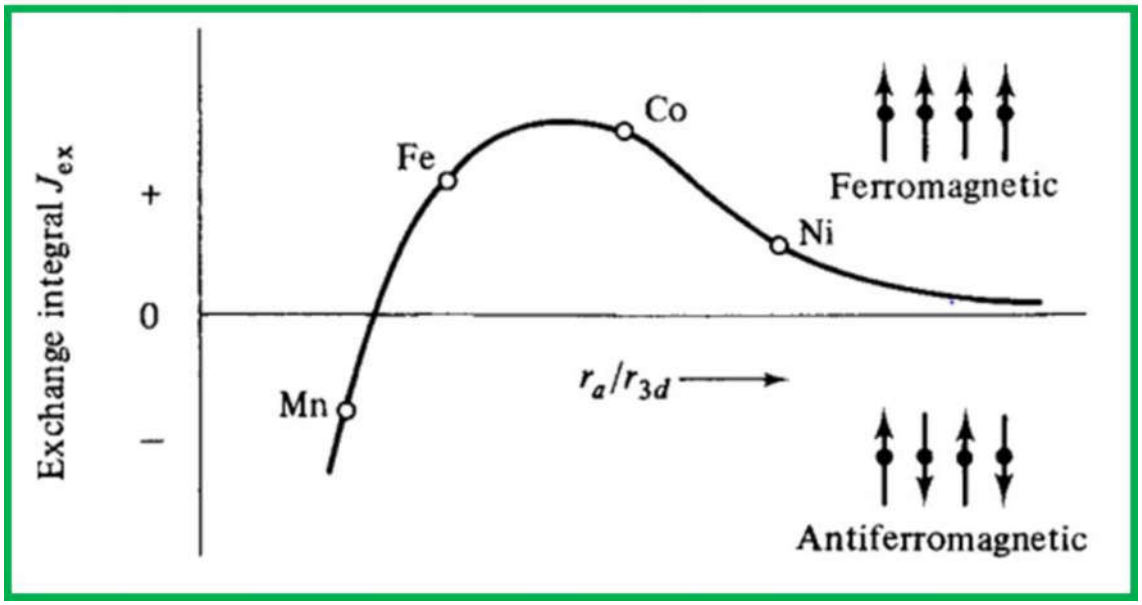

Figure 1.8 The Bethe-Slater curve: The variation of the exchange interaction with respect to the ratio of interatomic distance to the diameter of the 3d electron shell [20].

ordering with a positive exchange interaction. The nature of direct exchange interaction can be determined by referring to the Bethe-Slater curve, as depicted in figure 1.8.

1.3.2 Indirect exchange interaction

Direct exchange involves the interaction among adjacent magnetic moments, whereas in indirect interaction, the coupling between two neighboring cations is mediated by a shared non-magnetic ion, such as oxygen. In metals with localized electrons, such as rare earth metals with 4f electrons, the overlap of the wave functions involved in direct

exchange interaction is very small, and the indirect exchange interaction becomes the dominating mechanism for magnetic properties. In such cases, the magnetic ordering is caused by the indirect exchange interaction. The nature of magnetic coupling, whether it is ferromagnetic or anti-ferromagnetic, is decided by the separation between the magnetic ions interacting through indirect exchange.

1.3.2.1 Super exchange interaction

Super-exchange is a mechanism of magnetic interaction that occurs between neighboring magnetic ions through an intervening non-magnetic ion. A prominent example of this interaction is the coupling between the magnetic moments of two Mn^{3+} cations through an intervening non-magnetic oxygen (O^{2-}) anion. The strength and sign of the superexchange interaction depend on the occupation and orbital degeneracy of the magnetic ions involved. Goodenough extensively examined various scenarios of superexchange interactions, and their findings were summarized as the Goodenough-Kanamori rules [27–30]. Anderson later provided a simplified formulation that eliminates the need to consider the oxygen ion [31].

1. When the lobes of the singly occupied 3d orbitals of two metal (M) cations face each other, resulting in a large overlap, the exchange interaction is strong. This

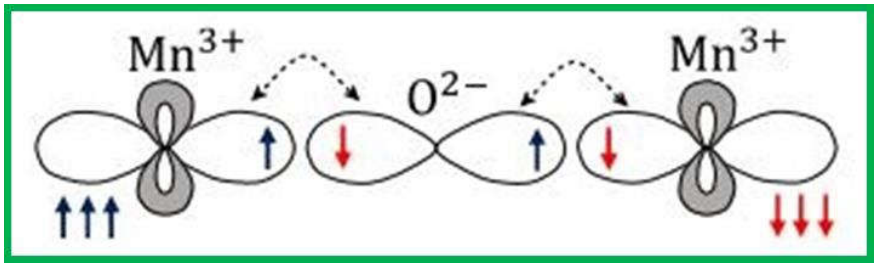

Figure 1.9 AFM in superexchange interaction

2. configuration leads to an antiferromagnetic interaction, which is commonly observed in M-O-M bonds with bond angles ranging from 120° to 180°, as shown in Figure 1.9.
3. In cases where the symmetry of the system causes the overlap integral between the singly occupied 3d orbitals of two metal (M) cations to be zero, the exchange interaction is relatively weak. This weak interaction gives rise to a ferromagnetic coupling, typically observed in M-O-M bonds with a bond angle of 90°, as illustrated in Figure 1.10.

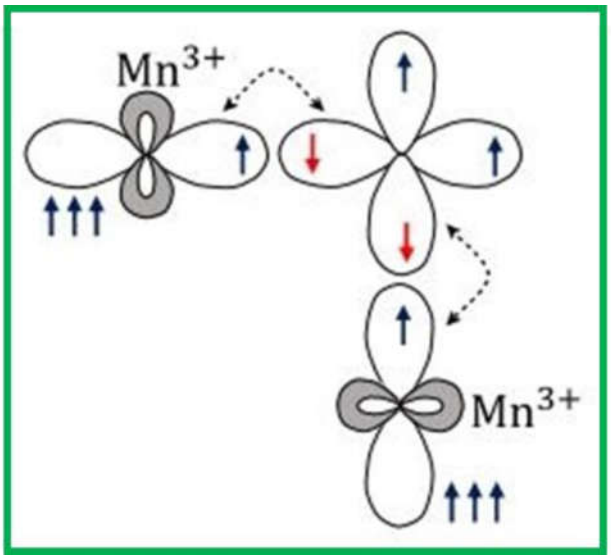

Figure 1.10 FM in superexchange interaction.

Overall, superexchange interactions between metal cations mediated through a non-magnetic anion are more commonly associated with antiferromagnetic behavior. This is primarily due to the larger overlap integrals, which are likely to be nonzero, and the bond angles (M - O - M) typically exceeding 90° [28].

1.3.2.2 Double exchange interaction

The double exchange interaction is a phenomenon that involves the interaction between magnetic moments of ions having mixed valence configurations. This concept was initially introduced by Zener in 1951 and can be understood as a type of super exchange interaction occurring between 3d atoms [32,33]. According to the Zener model, conduction electrons can hop between two ions only if the electron spins of the two ions are parallel [32,33]. In a system consisting of ions with different oxidation states, such as Mn^{3+} and Mn^{4+} ions illustrated in figure 1.11, the magnetic interaction between these ions mediated by oxygen (O2-) ions can be attributed to the double exchange interaction. This interaction involves the transfer of electrons from Mn^{3+} to oxygen and from oxygen to Mn^{4+} ions. If the spins of the Mn^{3+} and Mn^{4+} cations are parallel, the interaction between their electrons is ferromagnetic in nature. The transfer of electrons also relies on the bond angle of Mn-O-Mn, where a bond angle of 180 degrees corresponds to a strong interaction, while any deviation from 180 degrees leads to a weaker interaction. It is important to note that double exchange interaction always prefers ferromagnetism when the spins of manganese ions are parallel.

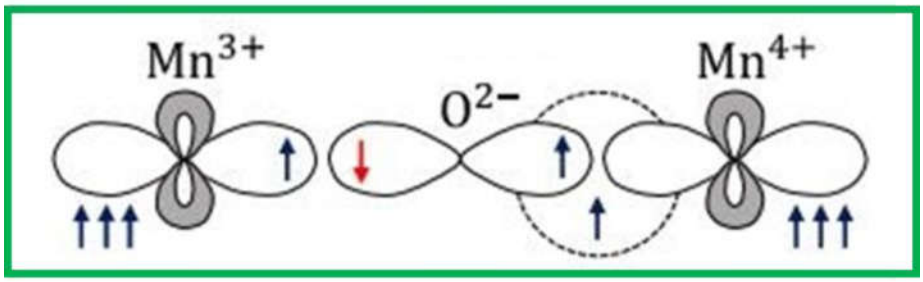

Figure 1.11 FM in double exchange interaction.

Conversely, the interaction becomes less favorable when the spins of manganese ions are antiparallel due to the onsite Hund's coupling making the electron transfer more difficult.

1.3.3 Dzyaloshinskii-Moriya interaction

In certain magnetic systems, the crystal symmetry promotes a canted spin arrangement rather than a fully antiparallel alignment of magnetic moments. As a result, weak ferromagnetism emerges within these antiferromagnetic systems. This phenomenon is facilitated by the Dzyaloshinskii-Moriya (DM) interaction, which is driven by spin-orbit coupling that produces excited states on one magnetic ion that interact with the ground state of another ion via exchange interactions. This interaction was first proposed by Igor Dzyaloshinskii [34] and later by Toru Moriya [35,36]. The DM interaction involves an antisymmetric exchange interaction between two neighboring magnetic spins via a non-magnetic ligand, expressed as

$$H_{DM} = D_{ij}.(S_i \times S_j) \qquad \text{--------- (1.5)}$$

where S_i and S_j are the spins of the two interacting magnetic ions, and D_{ij} is a DM constant proportional to the spin-orbit coupling constant and relies on the position of the ligand ion positioned between the two magnetic transition metal ions. The DM vector D_{ij} is oriented along the axis of symmetry. The DM interaction plays a crucial role in the orientation of magnetic moments in orthoferrites and orthochromites. Weak ferromagnetism in orthochromites is attributed to the DM interaction between magnetic ions. In perovskite ABO_3 structures, substitution in the A-site and B-site and a size mismatch between the A and B ions result in oxygen octahedral tilt and rotation, causing distortion. Consequently, each oxygen ion sandwiched between two neighboring B ions may shift away from the midpoint, creating a bent B-O-B bond that breaks the B-B axis rotation symmetry (as schematically shown in figure 1.12). This bent bond alters the DM interaction, which

becomes a relativistic correction to the super-exchange between magnetic B ions. Structural deformation and tilting caused by element substitution in perovskite alter the strength of the antisymmetric B-O-B exchange interactions.

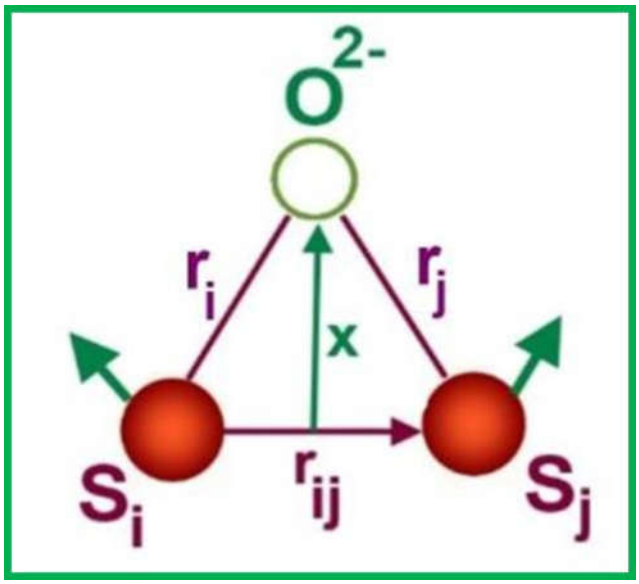

Figure 1.12 Schematic representation of DM interaction.

1.4 Exchange bias

Exchange bias (EB) is characterized by the asymmetric shift of a hysteresis curve away from the origin, as illustrated in Figure 1.13. This phenomenon was first identified in 1957 by Mieklejohn and Bean in Co particles [37]. It is associated with the anisotropy created at the interface between antiferromagnetic (AFM) and ferromagnetic (FM) materials. While conventional EB can be induced externally by field cooling (FC), internal factors can also contribute, and some systems even exhibit EB under zero field cooling (ZFC) conditions [38–40]. The magnitude of the exchange bias field (H_{EB}) is influenced by a range of intrinsic and extrinsic factors, including anisotropy, spin reorientation (SR), AFM layer thickness, AFM

domain structure, crystallinity, grain size, and interface impurity layers [38]. Above the Néel temperature (T_N), the EB field becomes zero and ceases to exist. In some instances, the EB disappears when the blocking temperature (T_B) is reached, which may coincide with T_N. While EB is commonly associated with AFM/FM interfaces, it has been observed in a variety of other systems, including AFM-ferrimagnet and FM-ferrimagnet interfaces, as well as in small particles, in homogeneous materials, metallic AFMs, thin films, ferrimagnets, oxide AFMs, and coated AFM single crystals [38,39]. In addition, EB has been observed in FM/FM interfaces of Ni-Fe-Co and Ni-Cu-Co sandwiches structure, which were characterized utilizing X-ray magnetic circular dichroism (XMCD) and magneto-optic Kerr effect (MOKE) [41]. In general, EB can be represented as follows:

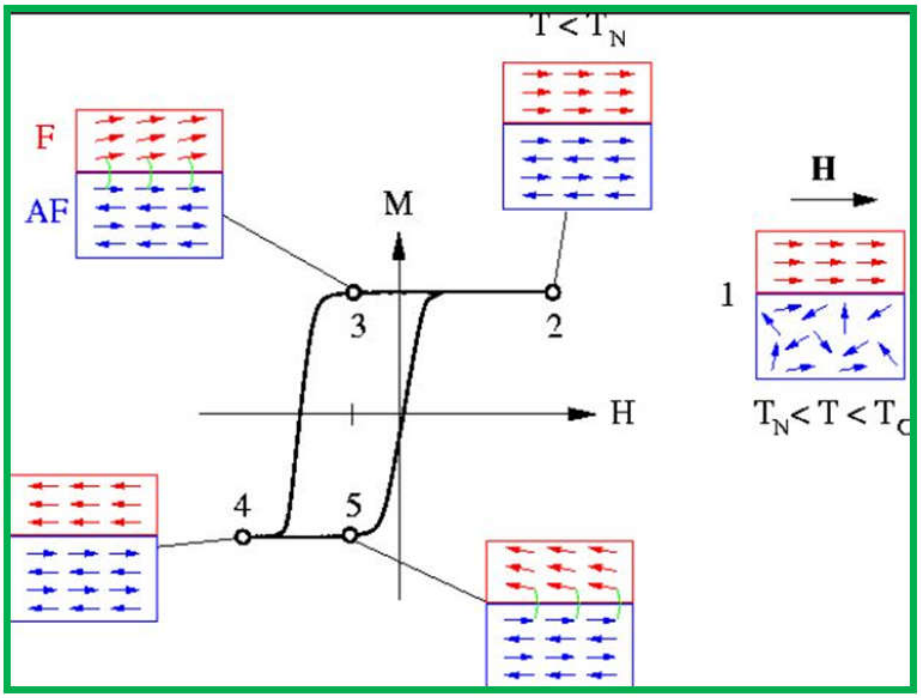

Figure 1.13 Diagram illustrating the spin configuration of a FM/AFM bilayer system, demonstrating the presence of the exchange bias effect.

Coercivity, cooling field, perpendicular coupling and Training effect, can be used to illustrate the qualitative information about the H_{EB} [40]. The EB can have a positive or negative effect depending on whether the easy axis of FM and AFM spins is parallel or perpendicular, respectively [42].

1.5 Rare earth orthochromites

$RCrO_3$ compounds, where R represents a rare earth element and Cr denotes chromium, have a crystal structure that is similar to rare earth ferrites and orthorhombic rare earth manganites [43]. These materials have a distorted orthorhombic structure and are classified as G-type antiferromagnetic with a magnetic ordering temperature that can range from around 110 K to 282 K [44–48]. The orthochromites exhibit a G-type configuration, specifically Γ_1, Γ_2, and Γ_4, as depicted in the figure 1.14 [43–49]. The magnetic structure of these compounds is determined by the magnetic character of the R-site element, with some exhibiting a magnetic structure that is represented by Γ_4 or Γ_2 [43–49]. However, certain $RCrO_3$ compounds experience a spin reorientation (SR) transition at low temperatures, which causes a change in their spin structure from Γ_2 to Γ_1 as a result of magnetic interactions between the R^{3+} and canted Cr^{3+} spins [50]. A few $RCrO_3$ compounds, including (Er, Sm, Gd, Nd) CrO_3, exhibit SR transitions that can be either continuous or discontinuous [47,48,51–53]. Apart from exhibiting multiferroic behavior, orthochromites also display interesting features such as negative magnetization (NM) just below the Cr^{3+} antiferromagnetic ordering temperature, along with weak ferromagnetism [47,49]. The resistivity plot of these compounds shows a break with temperature, indicating the possibility of ferroelectricity (FE) in $RCrO_3$. This was confirmed

by pyroelectric measurements, which were first discussed by Subba Rao et al. in the late 1960s [54].

Later studies by Tripathi and Lal showed that $RCrO_3$ are p-type semiconductors instead of insulators [55]. As $RCrO_3$ are centrosymmetric thus, ferroelectricity's genesis in these materials is still a matter of debate [49]. Various theories have been proposed, including local structural distortion, exchange striation between rare earth and chromium moments, and local symmetry breaking. However, the mechanism behind ferroelectricity in $RCrO_3$ remains unclear. $YCrO_3$ and $LuCrO_3$ have reported small polarization values of approximately 2 μC/cm2 and 0.35 μC/cm2, respectively [44,56]. A new concept regarding the origin of ferroelectricity in orthochromites was introduced in 2007, which emphasized the importance of local non- centro-symmetry [49]. This concept gained significant attention in the scientific community.

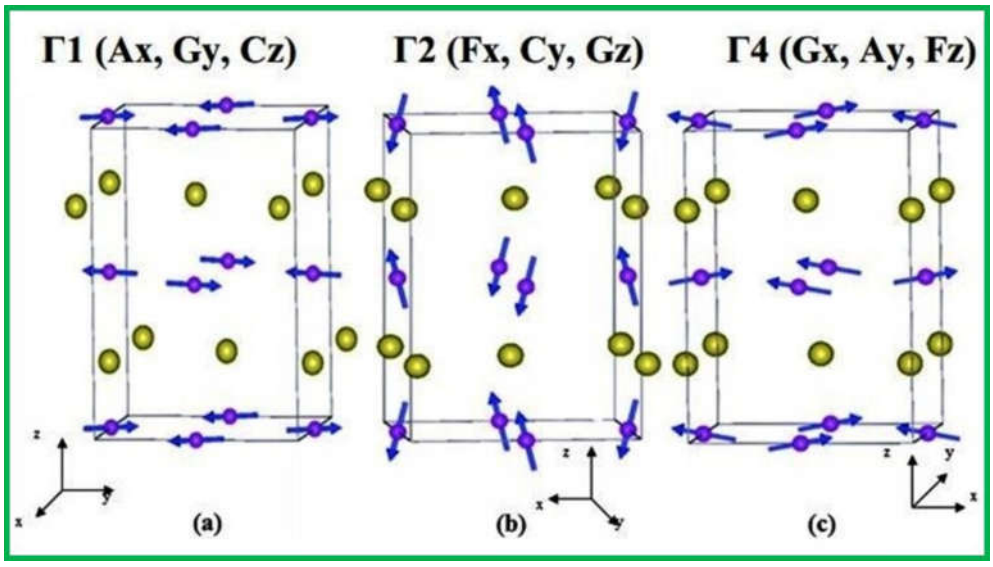

Figure 1.14 Within the G-type antiferromagnetic configuration, the spin structures Γ_1, Γ_2, and Γ_4 are manifested, exhibiting the Pbnm symmetry. [43,49] .

Future materials require multiple functionalities within a single phase. Recently, some $RCrO_3$ have demonstrated intriguing characteristics, such as negative magnetization (NM) and exchange bias (EB), which are technologically significant for spintronic and memory devices [39,47,57–61]. The challenge lies in studying the temperature and field induced NM and EB in single-phase $RCrO_3$, which remains unexplored until now. The pictorial diagram highlights main features of $RCrO_3$(Fig 1.15).

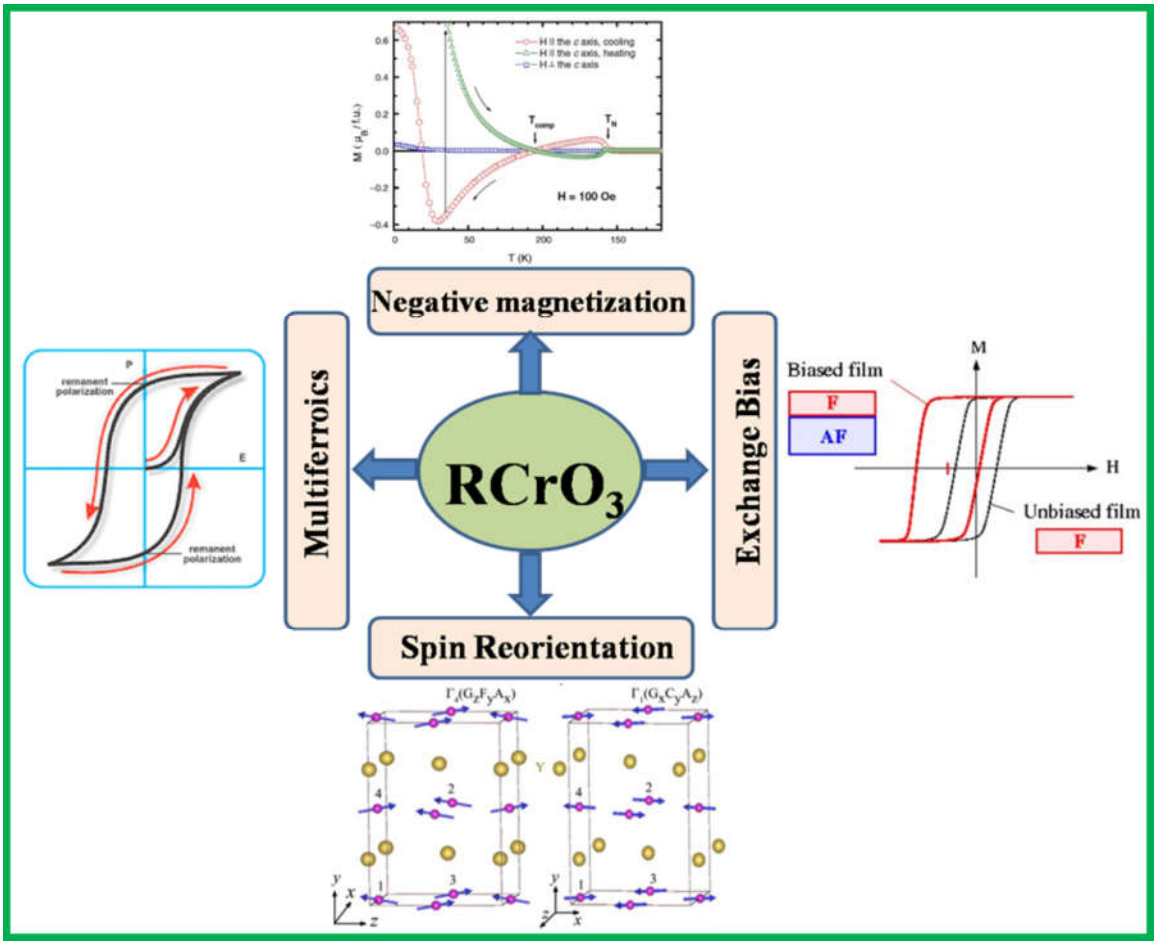

Figure 1.15 Pictorial diagram highlighting the unique characteristics of rare earth chromites.

NM can also be utilized to investigate the switching characteristics of the material. Moreover, despite the fact that the study of $RCrO_3$ has mostly focused on their multiferroic

properties, they are more accurately categorized as semiconductors as opposed to insulators [55]. This has sparked further interest in studying their utilization in photocatalysis and various light-harvesting applications, including solar photovoltaics. These materials offer a distinct advantage compared to conventional photocatalytic materials because their absorption bands generally lie in the visible range. The aforementioned characteristic, such as photocatalytic activity, NM, EB, and, magnetization switching have inspired us to investigate and explore the exceptional behavior displayed by $RCrO_3$.

1.5.1 Magnetization reversal/Negative magnetization

In the usual understanding of magnetization, materials such as PM, FM, and AFM are assumed to have positive magnetization, while diamagnetic materials have negative magnetization. However, there are certain types of magnetic materials that exhibit negative magnetization (NM), which does not arise from the diamagnetic contribution. This phenomenon, also known as magnetization reversal (MR), was initially discovered in spinel ferrites back in 1948 [62]. It occurs when the system is cooled to a low temperature while subjected to an external magnetic field or under zero-field cooled (ZFC) conditions. Conventionally, negative magnetization(NM) behavior is demonstrated when the system is cooled with the application of an external magnetic field (FC), but in some cases, ZFC magnetization shows the NM, as is the case with orthochromites [59,61]. This is a unique example of a complex phenomenon that is different for different systems. NM has been extensively detected and reported in various magnetic materials such as spinel ferrites, molecular magnets, perovskites, multilayers garnets, and intermetallic alloys [60–67]. Nonetheless, the understanding of NM remains a challenging and complex topic.

In the literature, potential explanations for NM behavior in magnetic materials have been classified into categories such as [39,61]:

(a) Negative exchange coupling among FM sublattices: In this case, negative magnetization has been observed in systems with different crystallographic sites due to an antiparallel ordering between two or more ferromagnetic sublattices. Spinel compound with the general formula AB_2O_4 exhibiting negative magnetization belongs to this category. For examples Co_2VO_4, Co_2TiO_4, Fe_2MoO_4 etc.

(b) Negative exchange coupling among canted AFM sublattices: Systems with canted antiferromagnetic (AFM) sublattices arranged antiparallel to one another at different crystallographic sites can also exhibit negative magnetization. Numerous perovskite compounds with the general formula ABO3 fall under this category. For example, (La, Y, Sm, Nd)VO_3, $BiFe_{0.5}Mn_{0.5}O_3$, $(Cr_{0.7}Ti_{0.3})_5S_6$,, $CaMn_{0.96}V_{0.04}O_3$ etc.

(c) Negative exchange coupling among FM/canted-AFM and PM sublattices: AFM and PM sublattices located at various crystallographic sites exhibit an antiparallel coupling in many systems, which is used to explain the presence of negative magnetization. Typically, in such cases, the paramagnetic atom at a crystallographic site encounters an effective negative molecular field generated by the neighboring ordered FM/canted-AFM sublattices. For instance, the MR is present in the case of $La_{1-x}Gd_xMnO_3$ (x = 0.25, 0.5, and 0.75) because the magnetism results from the intricate interaction of the 3d-4f orbital. Other example is $LaVO_3$, $CeVO_3$, $SmVO_3$, $GdCrO_3$, $ErCo_{0.5}Mn_{0.5}O_3$ and $NdVO_3$.

(d) Imbalance of spin and orbital moments: In this instance, systems with an antiparallel ordering between the spin and orbital moments of an atom or ion residing at a particular crystallographic site exhibit negative magnetization. These compounds have a cubic crystal structure of the the Laves-phase AB_2 type, also known as the C15 type with the Fd-3m space group, exhibits a diamond-like arrangement of A atoms and a tetrahedral arrangement of B atoms surrounding each A atom. For example, $(Sm_{1-x}Gd_x)Al_2$, Sm_2Al, SmNiAl etc.

(e) Interfacial exchange coupling between FM and AFM phases: The exchange coupled FM and AFM interfaces exhibit negative magnetization in the current instance due to the different temperature dependence of their magnetization. In these systems, the magnetic compensation actually takes place at mesoscopic levels (clusters/interfaces), not microscopic levels. For example, $NiFeF_2$, Gd-Fe, GdCo, Gd-CoNi multilayers, Fe_3O_4/Mn_3O_4 superlattice structures.

1.5.2 Magnetization reversal in pure and doped orthochromites

The negative magnetization (NM) behavior observed in $RCrO_3$ is primarily caused by the negative exchange coupling between the canted-antiferromagnetic (AFM) and ferromagnetic (FM) sublattices. $RCrO_3$ typically exhibit three dominant types of magnetic interactions: R^{3+}–R^{3+}, R^{3+}–Cr^{3+}, and Cr^{3+}–Cr^{3+}. The Cr^{3+} spins exhibit antiferromagnetic interaction through oxygen mediated interaction, which is the strongest interaction and occurs at a comparatively elevated temperature. In contrast, the R^{3+} spins start ordering at lower temperatures, below 10 K [47]. Other complex oxides such as $La_{1-x}Gd_xMnO_3$, $Nd_{0.96}Ce_{0.04}MnO_3$, $SmMnO_3$, $GdNi_{0.3}Mn_{0.7}O_3$, $GdCo_{0.3}Mn_{0.7}O_3$, etc., also exhibit NM

behavior [61,68–72]. In orthochromites, the NM behavior arises because the canted AFM spins induce an internal magnetic field on paramagnetic (PM) spins, which is greater than the applied magnetic field, resulting in NM behavior. This explanation also applies to $GdCrO_3$ [48,61,73], $YbCrO_3$ [74], $HoCrO_3$ [75,76], and $TmCrO_3$ [58] samples which exhibit NM behavior when the system is field-cooled under low external applied.

The $GdCrO_3$ nanoparticles exhibit two distinct T_{comp} (temperature points at which magnetization becomes zero) in addition to NM, which could be linked to the particles' core-shell structure. In contrast, in bulk, this phenomenon is believed to be caused by the antisymmetric D-M interaction. Likewise, the explanation for NM mentioned earlier is applicable to $YbCrO_3$ [74], $HoCrO_3$ [76,77], $TmCrO_3$ [58], and $SmFeO_3$ [78]. The temperature dependence of the sublattices in relation to the canted AFM Cr^{3+} spins in compounds like $La_{1-x}Pr_xCrO_3$ ($0.2 \leq x \leq 0.8$) [57,61,65], $La_{0.75}Nd_{0.25}CrO_3$ [59,61], $La_{0.5}Gd_{0.5}CrO_3$ [61,79], and $La_{0.1}Gd_{0.9}CrO_3$ [61,80] leads to NM. The NM/MR is generally observed in materials exhibiting a core-shell structure, undergoing structural transitions, possessing ferrimagnetic ordering between sublattices, experiencing extrinsic effects such as weak ferromagnetic clustering, and displaying a competition between single ion anisotropy and Dzyaloshinskii-Moriya (D-M) interaction. [34,36,59,61,76,78]. Therefore, considering the literature and understanding of NM, it is reasonable to anticipate the presence of NM in other $RCrO_3$. In a recent study, Lei et al. investigated $RCrO_3$ synthesized via hydrothermal method and observed NM in few $RCrO_3$[79].

1.5.3 Magnetization switching

The temperature driven magnetization reversal of has garnered significant interest for its potential utilization in thermomagnetic switches and devices for data storage [61]. Temperature induced NM has been demonstrated in various magnetic materials, such as orthoferrites, orthochromites, and, orthovanadates [58,65,74,81–85]. While it is well-known that the direction of applied external magnetic field can switch the magnetization, only a few systems exist where magnetization switching can be achieved by simply adjusting the temperature and the external applied magnetic field magnitude [58,82]. This requires the presence of more than one compensation temperatures (T_{comp}) in the magnetic materials. $TmCrO_3$, for instance, demonstrates magnetization switching (Figure 1.16(a)), where magnetization can be switched from negative to positive, below the T_{comp} by varying the externally applied magnetic field magnitude. The switching of magnetization observed in $TmCrO_3$ without changing the magnetic field direction provides a superior advantage compared to other magnetic materials for developing new memory devices [58,61].

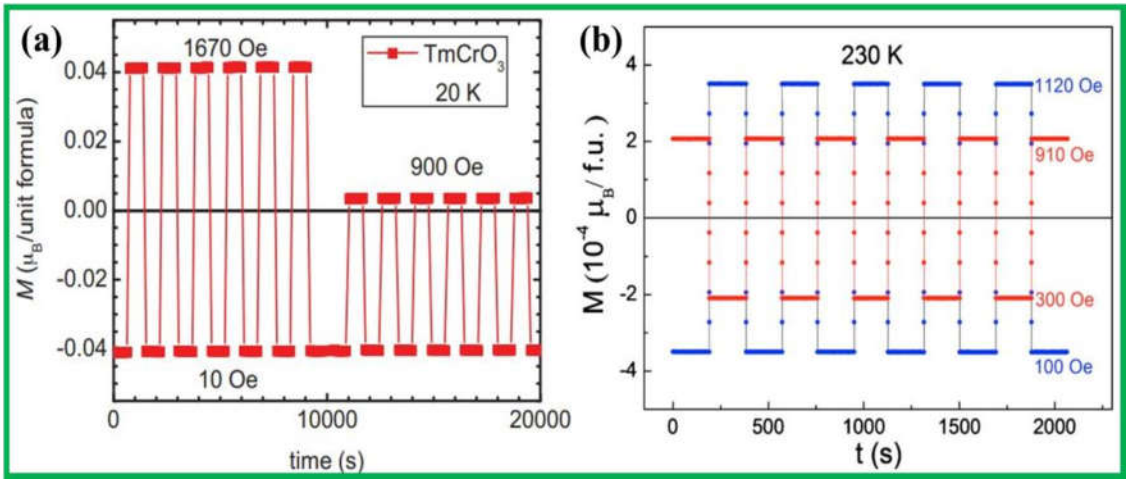

Figure 1.16 Field induced magnetization switching in **(a)**$TmCrO_3$ and **(b)** $YFe_{0.5}Cr_{0.5}O_3$

Similarly, $YFe_{0.5}Cr_{0.5}O_3$ displays magnetization switching (Fig1.16(b)) at 230 K under different applied magnetic fields [86]. This exceptional property has been observed in some

chromites, making them ideal candidates for developing non-volatile memories [61,81]. Since $RCrO_3$ is related to NM, the magnetization switching property is intriguing and distinctive, and warrants additional investigation for diverse applications, such as non-volatile memories and thermomagnetic switches. [38,39,61].

1.5.4 Exchange bias in orthochromites

Recently, some groups have observed EB in orthochromites, while others have not, which is still not fully understood [40,57,58]. Interestingly, the core-shell model is widely used to explain EB. Giri et al. put forward a model explaining exchange bias (EB) in $Sm_{0.5}Ca_{0.5}MnO_3$, which involves a core-shell structure. According to their proposal, the core is anticipated to exhibit antiferromagnetic (AFM) behavior, while the outer uncompensated spins constitute the shell [42]. Figure 1.18 shows a schematic for EB in the core-shell structure. Several systems, including $GdCrO_3$ [47,48], $TmCrO_3$ [58], $SmCr_{1-x}Fe_xO_3$[87], and $LaCr_{0.8}Mn_{0.2}O_3$ [59], have

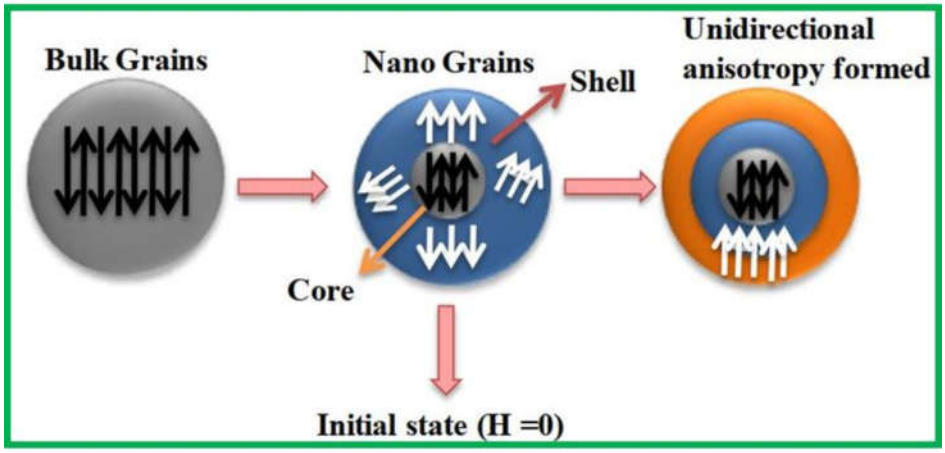

Figure 1.17 The diagram illustrating the phenomenological model for CO/AFM bulk manganites, including the corresponding nano grains. [42].

demonstrated both NM and tunable EB. However, $LaCrO_3$ has been widely investigated for its structural and magnetic characteristics in the orthochromites [46,88,89]. It is interesting to

note that EB is associated with NM, where H_{EB} = - M. While conventional field-cooled exchange bias (EB) is widely recognized, the occurrence of zero-field cooled EB has been documented in certain magnetic systems as a result of the presence of multiple phases within a single material. Initially, ZFC EB was thought to be a coincidental occurrence, but a model has been proposed for ZFC EB [40]. Most studies address positive/negative EB, and the tunability of EB is very rare. However, in the case of orthochromites, we can anticipate the tunability of exchange bias (EB) through variations in temperature and magnetization reversal, as some orthochromite have one or more T_{comp}.

1.6 Ce based chromite

Although rare earth orthochromites are popular perovskites and are well studied material, few reports are available in the literature on $CeCrO_3$ orthochromite [85,90,91]. It shows multifunctional behavior. Among these literatures, Shukla et al. for the first time report synthesis of $CeCrO_3$ of nanoparticles using a two-step combustion followed by calcination at 1223 K inside a vacuum-sealed quartz tube [90]. These synthesized nanoparticles exhibit a Néel temperature, T_N at approximately 257 K. Cao et al. synthesize bulk $CeCrO_3$ particles using arc melting method and observe the T_N at around 260 K [85]. Taheri et al. report the synthesis of $CeCrO_3$ through combustion combined with heat treatment at 1173 K under inert atmosphere and represent the T_N at 260 K also [91]. Among the $RCrO_3$ compounds, $CeCrO_3$ has the highest Néel temperature after $LaCrO_3$, which makes it desirable for applications near room temperature. Shukla et al. have reported negative magnetization (magnetization reversal) and a relaxor-like dielectric behavior of $CeCrO_3$ with an optical band gap of approximately 3.04 eV, indicating its potential for multifunctional applications [90]. The

reported optical band gap suggests that $CeCrO_3$ is suitable as a visible light-driven photocatalyst. Furthermore, $CeCrO_3$ and related compounds exhibit the exchange bias effect and sign reversal of exchange bias, making them applicable in various magnetic devices, including spin-valve devices, magnetic recording materials, and thermally assisted magnetic random-access memory [58,75,91]. Besides, $CeCrO_3$ shows negative magnetization with $T_N \sim 260$ K while $CeFeO_3$ shows a positive magnetization with high T_N above 620 K [85,90-95]. Recent report on $CeFeO_3$ shows a first order spin reorientation from Γ_4 to Γ_1 using neutron diffraction measurement while in $CeCrO_3$, second order spin reorientation from Γ_4 to Γ_2 is predicted by Cao et al [93,94]. Further, Shukla et al. and Taheri et al., have stated that $CeCrO_3$ exhibits a Γ_4 magnetic structure throughout the temperature range below T_N [90,91].

The detail investigation on magnetic structure of $CeCrO_3$ along with nuclear structure is not discussed in the literature. While few $RCrO_3$ compounds show positive magnetization, after substitution of Fe at Cr site, a negative magnetization under application of low external field is demonstrated. In particular, $LaCrO_3$ which shows positive magnetization, substitution of 5 at% of Fe at Cr site demonstrates negative magnetization which retains upto 15 at% of Fe [96]. Similarly, in $NdCrO_3$, the magnetization becomes negative after substitution of 5 at% of Fe at Cr site which persists upto 20 at% [97]. $RFeO_3$ and $RCrO_3$ compounds have been believed to possess p-type semiconducting behavior, to the best of our knowledge, detailed studies on band gap variation is not available in the literature neither on $CeFeO_3$ nor on $CeCrO_3$. Doping $CeCrO_3$ with Eu^{3+}, leads to a decrease in magnetization and reduction in T_N from 260 K to 178 K [93]. No reports show the effect of Fe dopant on $CeCrO_3$ where one may tune T_N, band

gap, exchange bias, magnetization orientation etc. which can enable to foresee the application mentioned above.

Therefore, it would be a matter of great interest to monitor the changes in optical band gap, magnetization behavior with temperature and field after substitution of Fe in $CeCrO_3$. Along with temperature dependent magnetic structure of $CeCrO_3$ which has not been confirmed in the literatures can be explored. Hence, in this thesis we examined the structure, optical and magnetic properties of $CeCr_{1-x}Fe_xO_3$ ($0 \leq x \leq 0.5$) compounds and predict the suitability for various applications like spin-valve, magnetic recording and thermally assisted magnetic random-access memory.

1.7 Objective

In this work, we have thus attempted to examine the change in structural, optical and magnetic properties after doping of Fe in $CeCrO_3$ where Fe(III) exhibits a higher ionic radius of 0.645 compared to Cr(III)'s ionic radius of 0.615, and also possesses a higher magnetic ground state moment of 5μB compared to Cr(III) with 3μB. It is also worth to mention that, due to super exchange interaction between Cr^{3+} and Fe^{3+}, there is a strong probability of superior magnetic property as predicted by Goodenough-Kanamori rule. Therefore, it would be a matter of great interest to explore the modification of structure, band gap and more importantly the magnetic properties including negative magnetization (magnetization reversal), exchange bias, Neel temperature with doping of Fe along with the magnetic structure of $CeCrO_3$. In this thesis, we explore the structural, optical and magnetic properties of $CeCrO_3$ with substituting the Fe concentration from 5 at % to 50at% and described in four different chapters.

Nano-crystalline, $CeCr_{1-x}Fe_xO_3(0 \leq x \leq 0.5)$ compounds synthesized by a facile one step nitrate-solution combustion method are crystallized in orthorhombic, *Pnma* structure. With the substitution of Fe in $CeCrO_3$, while the structural analysis demonstrates a linear increase in the lattice parameter and lattice volume with an increase in concentration from $x = 0$ to 0.5, the band gap reveals a linear decrease from 2.9 eV to 1 eV. Magnetization vs temperature analysis illustrates few exciting results such as Neel temperature which approaches more than 300K, persistence of negative magnetization upto $x = 0.07$, highest compensation temperature of 115K observed at $x= 0.05$ and two spin reorientation temperatures T_{SR1} and T_{SR2} for $x> 0.08$. Two spin reorientation temperatures are observed which increases from 43 K to 138 K and 23 K to 83 K, respectively with increase in x from 0.09 to 0.5. Further coercivity initially increases upto T_{SR1} and then decreases with increasing temperature for all samples. The highest coercivity i.e. 8.32 kOe is observed at 110 K for $x = 0.3$. We confirm from temperature dependent magnetic structure analysis using time of flight neutron diffraction data combined with magnetization measurement that Γ_4 (G_x, A_y, F_z) transform to Γ_2 (F_x, C_y, G_z) spin reorientation in $CeCrO_3$ nanoparticles. The field induced bipolar magnetization switching behavior observed for the first time in this system below T_{comp}, is a desirable parameter which can be opted for nonvolatile magnetic memory device application.